Highly anisotropic magnetoresistance of organic light-emitting diodes at geomagnetic field strengths

T. Grünbaum,[1] V. V. Mkhitaryan,[1] E. Schmid,[1] F. Dallinger,[1] S. Bange,[1] W. Jiang,[2] T. A. Darwish,[3] P. L. Burn,[2] and J. M. Lupton[1,*]

[1]*Institut für Experimentelle und Angewandte Physik, Universität Regensburg, Universitätsstraße 31, 93053 Regensburg, Germany*

[2]*Centre for Organic Photonics & Electronics, School of Chemistry and Molecular Biosciences, The University of Queensland, Brisbane, Queensland 4072, Australia*

[3]*National Deuteration Facility, Australian Nuclear Science and Technology Organization (ANSTO), Locked Bag 2001, Kirrawee DC, New South Wales 2232, Australia*

(Received 15 March 2022; revised 21 March 2023; accepted 24 May 2023; published 5 July 2023)

At geomagnetic field strengths, polymer organic light-emitting diodes (OLEDs) exhibit a giant anisotropy in magnetoresistance of up to 35%. Comparison of the effect arising from a protonated and an equivalent perdeuterated conjugated polymer, in combination with semiclassical quantum-stochastic modeling, demonstrates that microscopically anisotropic hyperfine-field distributions, on the level of the individual molecules, constitute the primary cause for this effect. For this microscopic anisotropy to emerge in the ensemble there must also be some degree of macroscopic ordering, which may arise from the structural anisotropy of the polymer. The theory predicts a critical field range, for which the anisotropy transitions from a twofold to a fourfold and back to a twofold angular functionality with increasing field strength, over a field range of only a few microtesla. Such a transition is indeed found experimentally, although it spans over a somewhat larger field range, suggesting a level of material disorder that is not accounted for in the simulations. Through the combination with microscopic modeling, anisotropic magnetoresistance can serve as a sensitive probe of macroscopic molecular ordering in organic semiconductors. The inclination compass effect in OLEDs also offers a potential route for probing the radical-pair mechanism of spin chemistry in the solid state, and the associated coherent and incoherent electronic and nuclear spin dynamics at room temperature, and could point to an intriguing analogy to some forms of avian magnetoreception.

DOI: 10.1103/PhysRevB.108.035201

I. INTRODUCTION

To explain the navigational abilities of some bird species, a spin-pair mechanism based on photoinduced electron transfer has been proposed and discussed widely in the literature [1–6]. This mechanism, originally developed to describe magnetic-field effects (MFEs) in chemical reactions [7–9], involves the creation of a radical pair and subsequent coherent spin precession—quantum oscillations—in local hyperfine fields. Such oscillations can lead to a mixing between singlet and triplet spin-pair configurations, the outcome of which is modified by a static magnetic field. Mixing is then followed by spin-dependent recombination with field-dependent reaction yields [8–10]. OLEDs offer a potential, if seemingly remote, analogy to radical-pair based MFEs [11], since their operation is also based on the capture and recombination of the spins of two charge carriers, electrically injected electrons and holes [12]. Both the resistance (R) and electroluminescence of OLEDs depend strongly on magnetic-field strength, down to the scale of a few hundred nanotesla [13,14], i.e., less than 1% of typical geomagnetic-field strengths. A weak but unexpected angular anisotropy in the magnetoresistance (MR) of OLEDs on the order of a few percent has previously been reported on the scale of several millitesla [15,16]. Although the field scale of this anisotropy lies two orders of magnitude above geomagnetic field strengths, such an anisotropy offers an important signature of a "spin-chemical compass" based on the radical-pair mechanism [17]: behavioral experiments on some birds indicate that they do not sense the *polarity* of the magnetic field but rather the *inclination* of the magnetic-field lines [18], which is inherently consistent with the radical-pair mechanism [17]. This earlier work on OLEDs is particularly interesting because there are actually only very few experimental reports of anisotropic MFEs in radical-pair systems to be found in the literature. This limitation arises from the fact that a macroscopically anisotropic MFE requires both a microscopic mechanism of anisotropy as well as macroscopic molecular ordering, which is lost in most solution-chemistry based experiments. In a recent report, an anisotropic MFE was indeed demonstrated in a bridged donor-acceptor complex in solution by using transient absorption spectroscopy [19]. An effective "ordering" of the molecules was imposed on the disordered system by selecting a particular orientational subset of molecules by using linearly polarized excitation [19].

As stressed by the authors of the earlier work on anisotropic MFEs in OLEDs in the magnetic-field regime $\geqslant$10 mT, it remained unclear whether the anisotropy originates from microscopic anisotropic hyperfine interactions of electronic and nuclear spins, or anisotropic dipolar spin-spin

*john.lupton@physik.uni-regensburg.de

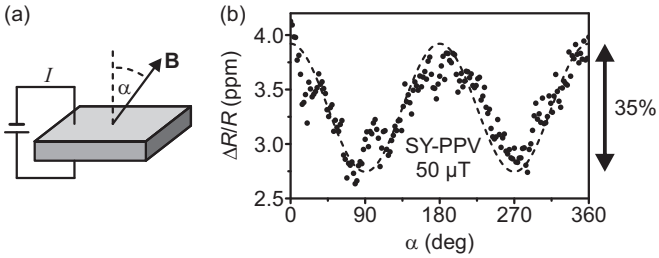

FIG. 1. Anisotropic magnetoresistance (MR) of SY-PPV OLEDs. (a) Schematic of the experiment. The OLED is operated with a constant current (5 μA) and the magnetic field is tilted with respect to the sample normal while keeping its magnitude constant. (b) For $B = 50$ μT, at a device current of 5 μA, relative MR exhibits an angular dependence with a 35% modulation. Dashed line shows a $\cos^2\alpha$ dependence.

coupling within the individual electron-hole carrier pairs [15]. In follow-up work, Cox *et al.* argued in favor of the anisotropic dipolar mechanism due to the observed angular dependence of the anisotropic MFE at 20 mT [16]. In addition, these authors considered the possible relation of the anisotropic MR to effects of spin-orbit coupling in the form of the Δg mechanism at fields greater than 200 mT, although this is generally very weak in organic semiconductors, and found it to be an unlikely scenario. To resolve this open controversy for the ultralow-field regime (i.e., below 1 mT), and explore the feasibility of anisotropic MR on geomagnetic-field scales, we have revisited this intriguing phenomenon with a material system in which the strength of the hyperfine interaction can be controlled directly [20].

II. EXPERIMENTAL PROCEDURE

Details of the device structure and the fabrication procedure are given in Sec. 1 of the Supplemental Material [21]. In brief, the OLEDs consist of an indium tin oxide-covered glass substrate, onto which a poly(styrenesulfonate):poly(3,4-ethylenedioxythiophene) layer is deposited by spin coating from water. The conjugated polymer material (approximately 70 nm) is subsequently spin coated from a toluene solution inside a nitrogen glove box, onto which a Ba/Al cathode is deposited by thermal evaporation. The samples are encapsulated inside the glove box and measured in air. The measurements presented in the following are performed by varying the angle α formed by the vector of the external magnetic field $\mathbf{B}$ with the sample normal $\hat{\mathbf{n}}$, as indicated in Fig. 1. With the aid of a three-dimensional arrangement of Helmholtz coils, measurements are performed for a fixed sample orientation with Earth's field compensated, so that only the direction but not the strength of the field changes (see Sec. 5 of the Supplemental Material [21] for details).

III. EXPERIMENTAL RESULTS

Following on from the work of Wagemans *et al.* [15], we examine the out-of-plane anisotropy of the MR at a magnetic field of $B = 50$ μT, close to Earth's field strength, for an OLED comprising an active layer of a soluble commercial poly(1,4-phenylenevinylene) (PPV) derivative, "Super Yellow

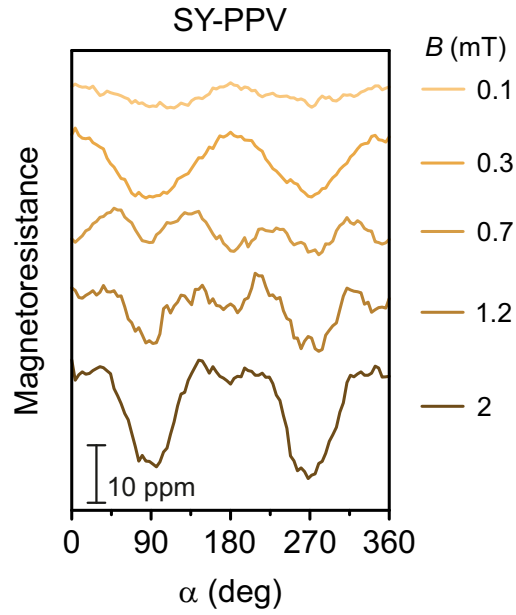

FIG. 2. Magnetic-field dependence of relative MR of SY-PPV OLEDs at a constant current of 5 μA for different magnetic-field strengths. Curves are offset for clarity.

PPV" (SY-PPV). Although the magnitude of MR, $\mathrm{MR} = \frac{\Delta R}{R} = \frac{R(B)-R(0)}{R(0)}$, at this field strength is only on the order of 4 ppm, varying the out-of-plane angle α results in a relative change in the MFE amplitude of $a = 2\frac{\mathrm{MR}(\alpha=0^\circ)-\mathrm{MR}(\alpha=90^\circ)}{|\mathrm{MR}(\alpha=0^\circ)+\mathrm{MR}(\alpha=90^\circ)|} = 35\%$ as plotted in Fig. 1(b). The anisotropy follows a $\cos^2\alpha$ dependence. This surprisingly large value observed for the MR anisotropy implies not only a high microscopic anisotropy of MFEs on the level of the individual molecules, or rather the individual charge-carrier pairs, but also a degree of anisotropic arrangement of the molecules on the bulk level—an isotropic arrangement of anisotropic spin pairs would average out in the ensemble. Such macroscopic structural anisotropy is usually studied in organic semiconductor films by examining the angular distribution of radiation intensities [22–24], by ellipsometry [25–27], or by grazing-incidence x-ray diffractometry [28]. Conjugated polymer chains tend to lie preferentially in the plane of the film. However, the origin of the microscopic anisotropy on the level of an individual electron-hole pair is more challenging to pinpoint: it may be due either to electron-hole spin-dipolar interactions or inherent to the hyperfine coupling. As discussed in Sec. 7 of the Supplemental Material [21], we find that the observed MR anisotropy is virtually independent of the current density and therefore of carrier density, suggesting that electronic spin-spin interactions are rather unlikely to be the source of the anisotropy.

A remarkable effect occurs when the magnetic-field dependence of the MR anisotropy is considered in Fig. 2. Varying the magnetic field from 0.1 to 2 mT affects the phase angle of the angular dependence of MR and also the functional form: it transitions from twofold modulation over 360° to fourfold and back to twofold. In addition, the degree of relative anisotropy, a, monotonically decreases from 35% at 50 μT to approximately 3% at 2 mT. Near-identical data are also

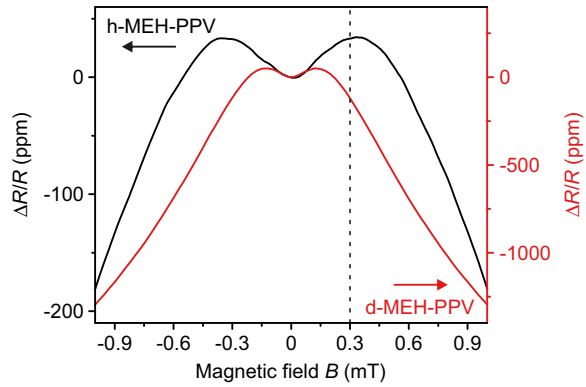

FIG. 3. Low-field MR of OLEDs based on h-MEH-PPV (black) and d-MEH-PPV (red). OLEDs were operated at a constant current of 10 μA (h-MEH-PPV) and 50 μA (d-MEH-PPV). Dashed line indicates $B = 300\,\mu$T as used for the anisotropy measurements in Fig. 4.

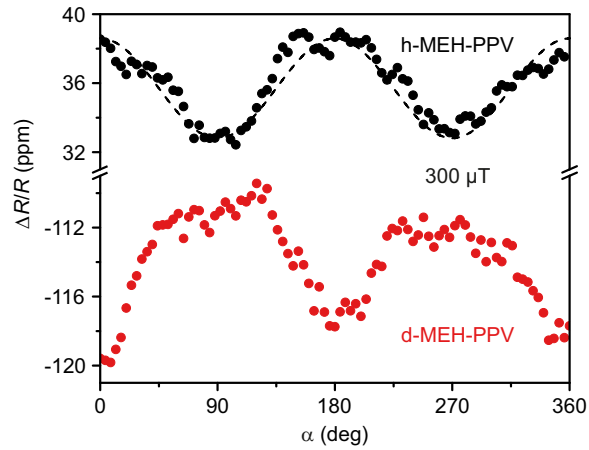

FIG. 4. Comparison of anisotropic MR for protonated and deuterated MEH-PPV-based OLEDs, operated under the same conditions as in Fig. 3. For an external magnetic field of $B = 300$ μT, an h-MEH-PPV OLED (black) exhibits orientation dependence of MR similar to that of SY-PPV, with cosine-squared dependence marked by a dashed line. d-MEH-PPV MR anisotropy (red), in contrast, has an opposite sign and appears somewhat distorted.

acquired under detection of the magnetic-field dependence of the anisotropy of the magnetoelectroluminescence, shown in Fig. S9 of the Supplemental Material [21].

In order to distinguish between contributions of anisotropic hyperfine and dipole-dipole interactions to the anisotropy, we compare OLEDs made of materials that differ only in the strength of hyperfine coupling. We recently introduced a perdeuterated version of the well-known poly[2-methoxy-5-(2'-ethylhexyloxy)-1,4-phenylenevinylene] (MEH-PPV), in which 97% of the hydrogen atoms are replaced by deuterium [20], whereas commercial SY-PPV contains only protons. The optical and electronic properties of the two compounds, protonated h-MEH-PPV and deuterated d-MEH-PPV, such as emission spectra and current-voltage characteristics, are virtually identical, as shown in Fig. S1 [21]. Figure 3 compares the MR curves for the two materials [20,29]. Since the hyperfine-coupling constant of deuterium is 6.5 times smaller than for hydrogen, and the spin of deuterium is $I = 1$, in contrast to $I = 1/2$ of the proton, the standard deviations of (random) effective hyperfine fields are reduced by a factor of ~ 4 in d-MEH-PPV [20,29]. Correspondingly, the magnetoresistance profile of d-MEH-PPV is considerably narrower than that of h-MEH-PPV since the hyperfine-field induced spin mixing is suppressed more easily by an external magnetic field [30]. The dashed line in the graph marks the magnetic-field value of $B = 300$ μT used in the subsequent anisotropy measurements in Fig. 4. It is important to note that because of the difference in the widths of the two magnetoresistance profiles, the *absolute* signs of the magnetoresistance at this value of B are opposite for h-MEH-PPV and d-MEH-PPV.

Figure 4 shows the MR anisotropy for OLEDs made of the two materials, measured at $B = 300$ μT. As expected, the signs of the MR amplitude are opposite, but, surprisingly, the functional form of the two curves appears different. Whereas the anisotropy for h-MEH-PPV appears to follow the cosine-squared dependence also seen in Fig. 1, the anisotropy for d-MEH-PPV appears to deviate somewhat from this dependence, tending towards the fourfold modulation seen at $B = 700$ μT for SY-PPV in Fig. 2. The definition of the relative anisotropy a infers an effective sign of the twofold anisotropy, which depends on whether $\mathrm{MR}(\alpha = 0^\circ) > \mathrm{MR}(\alpha = 90^\circ)$ (positive) or $\mathrm{MR}(\alpha = 0^\circ) < \mathrm{MR}(\alpha = 90^\circ)$ (negative). Crucially, this sign of anisotropy, which is not directly related to the sign of the MR, is opposite between d-MEH-PPV and h-MEH-PPV devices at low-field values.

Figure 5 shows the magnetic-field dependence of the anisotropy for the protonated and deuterated MEH-PPV. As for the case of SY-PPV in Fig. 2, a change with field in the functionality of the dependence is observed. Even though the electrical and optical characteristics of the two MEH-PPV compounds are virtually identical, the functional form of the anisotropy appears to differ. Remarkably, we find that for h-MEH-PPV and SY-PPV, the sign of the anisotropy is the same for 0.3 and 2 mT, i.e., in the two regions of twofold symmetry, but inverted comparing these two field regions in the case of d-MEH-PPV. The fact that deuteration has such

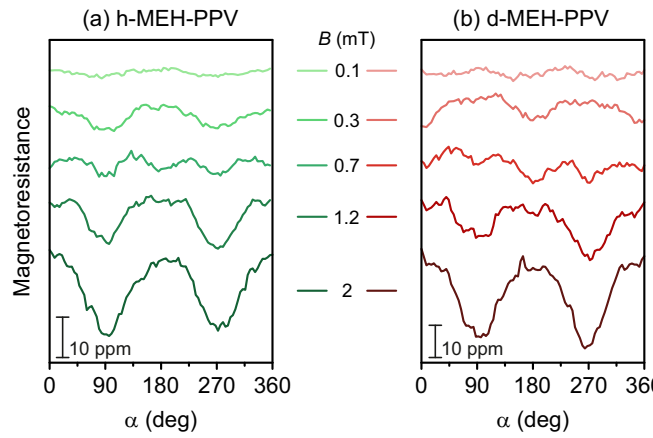

FIG. 5. Magnetic-field dependence of relative MR of (a) h-MEH-PPV and (b) d-MEH-PPV OLEDs for different magnetic-field strengths. Curves are offset for clarity.

a dramatic effect on the MR anisotropy clearly demonstrates that the anisotropic hyperfine interactions are important for the overall microscopic anisotropy.

Finally, we note that close inspection of Figs. 1, 2, 4, and 5 reveals that the maxima and minima within one sweep over 360° are not exactly the same height, indicating a degree of systematic unidirectional anisotropy in the experiment. We do not attach much significance to this observation and speculate that it arises primarily from an incomplete compensation of the geomagnetic field. A detailed discussion of this aspect is provided in Sec. 6 of the Supplemental Material [21].

IV. QUANTUM-STOCHASTIC SIMULATIONS

The fact that the magnetic-field dependence of the MR anisotropy differs for h-MEH-PPV and d-MEH-PPV suggests that the hyperfine coupling, and therefore the microscopic anisotropic hyperfine interaction, could be responsible for the observed anisotropy effect, but it does not allow an assessment of the possible role of anisotropic dipolar spin-spin interactions. In order to distinguish between these two possible microscopic causes of anisotropy, we simulate the dynamics of the spin-pair system by solving the stochastic Liouville equation for the evolution of the spin-pair density matrix [15,31–33] in Liouville space [34]. Details of the simulations are given in Sec. 4 of the Supplemental Material [21], along with a critical discussion of the choice of parameters and the implications thereof. In brief, we account for the microscopic anisotropy by describing the hyperfine interaction semiclassically as local static random magnetic fields, i.e., originating from a Gaussian distribution with zero mean, independent from site to site [35]. Characteristic magnitudes of random hyperfine fields acting on electron and hole spins generally differ [29,36]. With the assumption of isotropic hyperfine interactions, the Cartesian components of local hyperfine fields, $B_{i,\nu}$—with $i = x', y', z'$ and $\nu = \mathrm{e}, \mathrm{h}$ labelling electrons and holes, respectively—are drawn from a Gaussian distribution, $\mathcal{N}(B_{i,\nu}) = (2\pi b_{\mathrm{hyp},\nu}^2)^{-1/2} \exp(-B_{i,\nu}^2/2b_{\mathrm{hyp},\nu}^2)$. Here, $b_{\mathrm{hyp},\nu}$ denotes the standard deviation of the hyperfine-field components experienced by charge-carrier species ν. The resulting hyperfine Hamiltonian of a spin pair reads $H_{\mathrm{hyp}} = \hbar\gamma(\mathbf{B}_\mathrm{e}\mathbf{S}_\mathrm{e} + \mathbf{B}_\mathrm{h}\mathbf{S}_\mathrm{h})$, where γ is the electron (and hole) gyromagnetic ratio and $\mathbf{S}_\mathrm{e}$, $\mathbf{S}_\mathrm{h}$ are the spin operators of electron and hole. We consider a hyperfine interaction with axial anisotropy quantified by the real positive parameter η, the same for electrons and holes. This axial anisotropy is defined relative to the local system of molecular axes (x', y', z') and is introduced by rescaling the standard deviations along the local molecular axes, $b_{\mathrm{hyp},x',\nu} = b_{\mathrm{hyp},\nu}/N_\eta$, $b_{\mathrm{hyp},y',\nu} = b_{\mathrm{hyp},\nu}/N_\eta$, and $b_{\mathrm{hyp},z',\nu} = \eta b_{\mathrm{hyp},\nu}/N_\eta$, with $N_\eta = (2/3 + \eta^2/3)^{1/2}$. Because of axial symmetry, this anisotropic hyperfine interaction is determined locally by the orientation of the molecular z' axis. In the general case, these z' axes are oriented randomly throughout the ensemble of spin pairs, independently for individual electron and hole spins.

Besides the hyperfine and Zeeman interactions, electron and hole spins within the pair also interact with one another. This coupling has two components, dipolar and exchange. The dipolar coupling is determined by the intrinsically anisotropic Hamiltonian, $H_{\mathrm{dip}} = D[\mathbf{S}_\mathrm{e}\mathbf{S}_\mathrm{h} - 3(\mathbf{S}_\mathrm{e}\mathbf{r})(\mathbf{S}_\mathrm{h}\mathbf{r})/r^2]$, where $\mathbf{r}$ is the displacement vector connecting electron and hole spins and $D = \mu_0\hbar^2\gamma^2/4\pi r^3$ is the dipolar coupling strength in the point-dipole approximation, with μ_0 the vacuum permeability. The exchange coupling is described by the Hamiltonian $H_{\mathrm{exc}} = -J\mathbf{S}_\mathrm{e}\mathbf{S}_\mathrm{h}$, assuming isotropy. Experimental estimates for the scale of J and D in electron-hole pairs in conjugated polymers have previously been reported as $|J| < 30$ neV and $|D| = 23.5 \pm 1.5$ neV based on magnetic resonance spectroscopy [20,37].

For the microscopic anisotropy of either the hyperfine-field distributions or the dipolar interaction to translate into an observable MR(B, α), finite macroscopic ordering of the π-conjugated segments that host the charges in the bulk film is required. One way to account for this order is to introduce a distribution function $P_\pm(u) = P_{\varepsilon\pm}\frac{1}{1\pm\varepsilon^2u^2}$ for the orientation $u = \cos(\theta)$ of the local molecular z' axes and the intrapair displacement vectors $\mathbf{r}$ with respect to the sample normal, where the degree of macroscopic ordering is determined by the parameter ε, with $\varepsilon = 0$ corresponding to the isotropic case. Here, the plus sign yields a distribution of θ predominantly around 90° (i.e., around the sample plane), whereas the minus sign gives a distribution dominated by the regions around the sample normal, i.e., close to $\theta = 0°$ and $\theta = 180°$. Visualizations for various cases of $P_\pm(u)$ and the definition of the normalization constant $P_{\varepsilon\pm}$ are given in Sec. 4 of the Supplemental Material [21]. Since the distributions of z' and $\mathbf{r}$ are not necessarily correlated [38,39], separate order parameters $\varepsilon_{\mathrm{hyp}}$ and $\varepsilon_{\mathrm{dip}}$ are introduced for hyperfine and dipolar contributions. *Monte Carlo* sampling is then used to average over the different realizations. Thus, the simulation accounts for both microscopic and macroscopic anisotropy, involving computational experiments on the single-molecule level which are averaged over an ensemble corresponding to the bulk level.

We chose d-MEH-PPV to model the MFE anisotropy for the two proposed mechanisms, since this material has the lowest level of hyperfine-field disorder, quantified accurately by magnetic resonance spectroscopy [20], and because the spin-1 of the deuterium nuclei can be considered to behave somewhat more "classically" than the spin-½ of the protium nuclei and is thus easier to treat in the semiclassical approach used here (cf. the discussion in Sec. 4.6 of the Supplemental Material [21]). As parameters characterizing the interaction of electronic spins with nuclear and other electronic spins, we take the experimental values $b_{\mathrm{hyp,e}} = 0.288$ mT and $b_{\mathrm{hyp,h}} = 0.091$ mT [20,29]. As detailed in Supplemental Material, Fig. S2 [21], optimal fitting to experiment is found for $D = 6.95$ neV (i.e., 60 μT) and $J = 19.7$ neV (i.e., 170 μT). A discussion of the robustness of the result of the model to the choice of parameters, in particular the perhaps surprising relation $J > D$, is given in Sec. 4.5 of the Supplemental Material [21]. It should be stressed that the set of values chosen is not necessarily unique; rather, values are chosen to optimize fits to the MR curves and to reproduce the anisotropy. To distinguish between the influence of molecular-scale anisotropies related to either dipolar electronic spin-spin or hyperfine interactions, we consider extreme realizations of the two scenarios: (1) fully oriented molecular z' axes

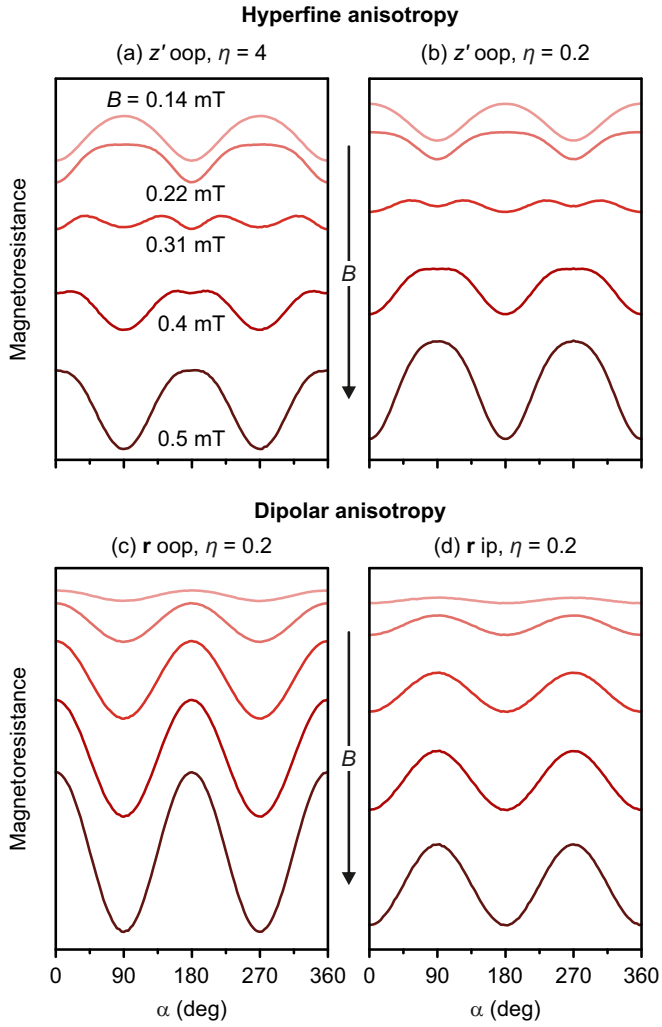

FIG. 6. Simulations of MR anisotropy of d-MEH-PPV OLEDs for extreme cases of either only anisotropic hyperfine interactions (a), (b) or only anisotropic electron-hole dipolar interactions (c), (d). In (a), (b), MR anisotropy is shown for two values of microscopic anisotropy parameter η, with all z' axes pointing in the out-of-plane direction. Panels (c), (d) display results for out-of-plane and in-plane orientations of electron-hole pair displacement vector **r**. While the first two cases show a transition in symmetry of angular dependence with increasing field, in agreement with experiment, the latter do not. Curves are plotted on an arbitrary scale and offset vertically to appear ordered according to the values of the external magnetic field as stated in panel (a). Detailed information on the simulation parameters is given in the Supplemental Material [21].

together with isotropic spin-pair displacement vectors **r** (i.e., a purely "hyperfine anisotropy"); and (2) isotropic molecular axes combined with fully oriented displacement vectors (i.e., a purely "dipolar anisotropy"). For case (1), the simulations were performed for two values of the microscopic hyperfine anisotropy, $\eta = 0.2$ and 4. These values are chosen for optimal reproduction of the measured MR curves. Figure 6 shows the model results for different conditions. Each panel displays angle-dependent MR for five values of B. In panels 6(a) and 6(b), the z' axes are oriented along the sample normal $\hat{\mathbf{n}}$, whereas the displacement vectors are distributed isotropically. In both cases, a striking transition from twofold to fourfold to twofold symmetry of MR(α) is observed with increasing field strength. Such an evolution is also identified experimentally for all three materials investigated in Figs. 2 and 5, and is even seen in the anisotropic magnetoelectroluminescence shown in Supplemental Material, Fig. S9 [21]. Provided that the hyperfine fields are assumed to be greater along the out-of-plane direction [Fig. 6(a)], the calculated MR anisotropy is in good qualitative agreement with experiment as seen in Fig. 5(b). Nevertheless, there are differences in the range of magnetic field values for which the transition between two- and fourfold symmetry occurs. These differences may be a result of the shortcomings of the semiclassical model as discussed in Sec. 4.6 of the Supplemental Material [21], or point to the involvement of additional sources of anisotropy, such as the dipolar anisotropy. If, however, the origin of the MR anisotropy is restricted solely to an anisotropic distribution of displacement vectors **r**, as in panels (c) and (d) of Fig. 6, i.e., if the distribution of hyperfine interactions is isotropic in the ensemble, the striking evolution of the functional form of MR(α) with increasing field is lost [40]. The experimental observation that anisotropic hyperfine-field distributions are the primary reason for anisotropic MR is therefore corroborated by the simulations.

V. COMPARISON OF EXPERIMENT AND THEORY

As a final step, we attempt to model the measured MR anisotropy *quantitatively*. To do so, we choose $\eta = 4$ and vary $\varepsilon_{\mathrm{hyp}}$ and $\varepsilon_{\mathrm{dip}}$ to match the experimental observations, i.e., we have to employ both hyperfine and dipolar anisotropy to fit the data. Close agreement arises for $\varepsilon_{\mathrm{hyp}} = 0.65$ and $\varepsilon_{\mathrm{dip}} = 0.58$, where the z' axes are distributed predominantly out of plane [$P_-(u)$] and the intrapair displacement vectors **r** lie predominantly in plane [$P_+(u)$]. The remaining parameters are identical to those used above. In Fig. 7, the simulated and measured anisotropy in MR are compared for three values of magnetic-field strength. The MR values for the midpoint and the perimeter of the polar plots are stated in the figure caption and a scale bar indicates the total variation in amplitude observed. The sign change of the relative anisotropy a observed in the measurements shown in Fig. 5(b) manifests as a rotation of the polar plot by 90° in Fig. 7. In all cases, excellent qualitative agreement of the angular pattern is found with a reasonably close match of the magnetic-field strength for which the transition in symmetry occurs. For $B = 0.3$ mT and $B = 2$ mT, the degree of relative anisotropy observed in experiment is reproduced almost quantitatively by simulation. At $B = 0.3$ mT, the relative anisotropy is $a = -6.3\%$ in both experiment and simulation, whereas at $B = 2$ mT, the simulation overestimates the experimental value ($a = 1.2\%$) roughly twofold. The experimental magnetic-field strength around which the transition in symmetry occurs is $B = 0.7$ mT, whereas the simulation predicts it at a field approximately 50 μT stronger. In the region of fourfold symmetry of the MR anisotropy, the experimental relative anisotropy ($a' = -0.6\%$) is substantially underestimated by theory ($a' = -0.02\%$) [41]. These deviations need not necessarily be a sign of a general shortcoming of the model, although they may relate to

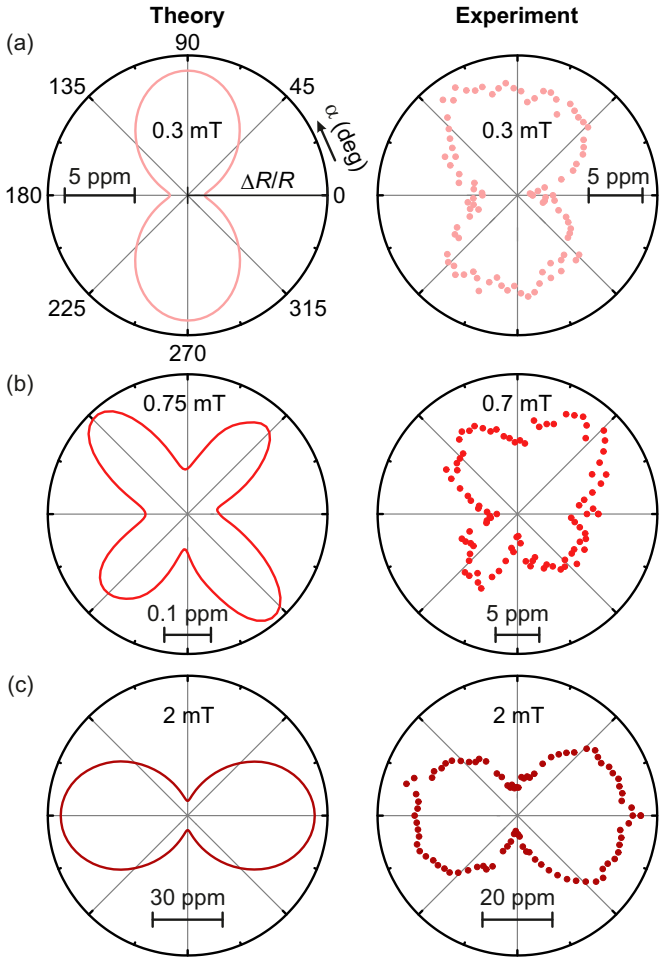

FIG. 7. Comparison of the simulated MR anisotropy of d-MEH-PPV OLEDs with experimental results. Data are displayed in polar plots for three magnetic fields. MR values for center (c) and perimeter (p) of each polar plot are (a) sim.: $MR_c = -125$ ppm, $MR_p = -115$ ppm; exp.: $MR_c = -121$ ppm, $MR_p = -108$ ppm; (b) sim.: $MR_c = -943.8$ ppm, $MR_p = -943.5$ ppm; exp.: $MR_c = -866$ ppm, $MR_p = -850$ ppm; and (c) sim.: $MR_c = -2150$ ppm, $MR_p = -2090$ ppm; exp.: $MR_c = -2110$ ppm, $MR_p = -2070$ ppm.

the general limitations of the semiclassical approach used as discussed in Sec. 4.6 of the Supplemental Material [21]. Crucially, the simulations in Figs. 6(a) and 6(b) yield comparable levels of anisotropy for the regions of both twofold and fourfold symmetry. The slight deviations between measurement and model may conceivably arise from the fact that the model does not capture all possible relevant contributions to MR. An obvious model limitation is the empirically chosen combination of the value of the microscopic hyperfine-induced anisotropy, η, and the macroscopic ordering of z' axes, $\varepsilon_{\mathrm{hyp}}$. η not only affects the magnitude of the angular dependence but also the functional shape of MR. In addition, it is likely that the macroscopic anisotropy in OLEDs is of a form more complicated than that in terms of a single-parameter distribution $P_{\pm}(u)$, e.g., given by a distribution in $\varepsilon_{\mathrm{hyp}}$ across the OLED active layer corresponding to local variations in microscopic order.

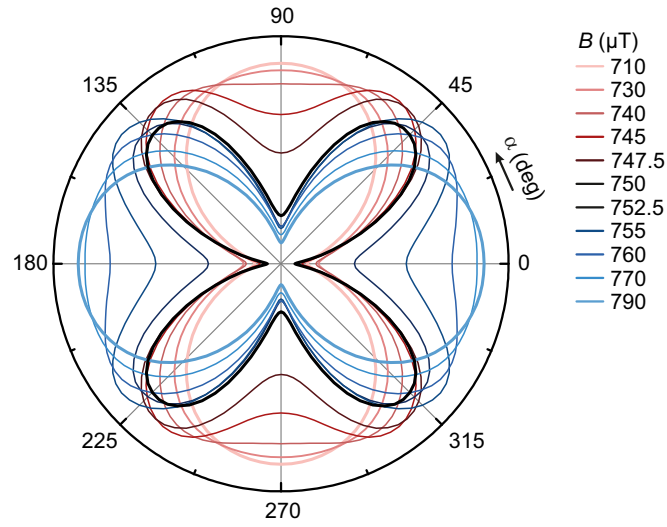

FIG. 8. Simulated, normalized MR anisotropy of d-MEH-PPV OLEDs for 11 magnetic-field values in region of symmetry transition of MR functionality close to $B = 0.75$ mT. See the Supplemental Video [21] for an animation of the evolution of the MR anisotropy.

To further elucidate the transition between twofold and fourfold symmetry of the angular MR dependence with magnetic field, we performed additional MR simulations in the transition region. Figure 8 shows polar plots of $\mathrm{MR}(\alpha)$ simulated for 11 different magnetic-field strengths around the value of $B = 0.75$ mT at which the fourfold symmetry is virtually ideal. An animation of this evolution is also shown in the Supplemental Video [21]. The plots are normalized to their maximal amplitudes. At $B = 0.71$ mT and $B = 0.79$ mT, pure twofold symmetries in the angular functionalities are observed, albeit rotated by 90°. This rotation and the transition in and out of the fourfold symmetry occurs over a field scale of 80 μT, i.e., comparable to geomagnetic-field strengths. Substantial changes in the functionality of the $\mathrm{MR}(\alpha)$ plot are discernible on field scales of a few microtesla around a field strength of 750 μT at near-perfect fourfold symmetry. The field region for which the fourfold symmetry is observed is hence extremely narrow, and even the slightest variations in parameters will affect the overall $\mathrm{MR}(\alpha)$ functionality.

Once again comparing the experimental results in Figs. 5 and 7 with simulations in Figs. 6, 7, and 8, we note that the change in the symmetry (twofold to fourfold to twofold) and the sign of anisotropy cannot be reproduced by dipolar anisotropy but rather is caused by the hyperfine anisotropy. Still, to fit to experiments, both dipolar and hyperfine anisotropy contributions are necessary.

VI. DISCUSSION AND OUTLOOK

Besides the aforementioned slight discrepancies, agreement between theory and experiment is quite compelling. The results of the simulations are consistent with our experimentally founded hypothesis that anisotropic hyperfine-field distributions are the dominant cause of the anisotropic MFEs, in contrast to earlier conclusions drawn from measurements at much higher fields [16]. We do note, however, that so

far, we have not been able to model the entire field range of anisotropic MR for h-MEH-PPV and SY-PPV. In part, we attribute this failure to the presence of further contributions to the MFE in OLEDs not accounted for here, such as the quenching of triplet excitons by charge carriers [42]. However, deviations between theory and experiment may also arise from additional sources of anisotropy, such as anisotropic rates of carrier-pair formation by Coulombic capture, owing to the anisotropic dielectric tensor, and hence anisotropic rates of recombination, dissociation, or even spin relaxation. In particular, it has previously been speculated that these rates may correlate with the direction of the electric field applied to the OLED, which could induce an additional asymmetry [15]. In addition, the macroscopic anisotropy will vary throughout the polymer film of the device, giving rise to additional disorder not accounted for in the model; this may be the reason why the symmetry transition is so much sharper in the simulations (Fig. 8) than what is seen in experiment. Also, we have assumed equal anisotropic interactions for electrons and holes, which is invariably only a necessary approximation; electron and hole wave functions in MEH-PPV are known to experience different hyperfine-field distributions [36].

Although MR and magnetoelectroluminescence, which probes spin-dependent recombination more directly than MR, appear to follow the same anisotropy as a function of magnetic field (see Supplemental Material, Fig. S9 [21]), it may be possible to learn more about additional sources of anisotropy by a more detailed comparison of the two observables, particularly as a function of temperature, by which contributions from spin-dependent recombination and transport can be distinguished [43]. We note, however, that the radical-pair model itself is inherently independent of temperature since it relies on changes of the spin permutation symmetry of the pair rather than magnetic-field induced Zeeman splitting; as a consequence, direct measurements of the spin coherence time within the pair by electrically detected magnetic resonant spin-echo spectroscopy have shown that it is virtually temperature independent [44]. We also point out in Sec. 4.6 of the Supplemental Material [21] the limitations of the semiclassical approach used here and discuss some of the potential benefits of a more complete quantum-mechanical model of the spin-spin interactions such as those described in Ref. [45]. We stress, nevertheless, that the semiclassical model appears to succeed in capturing the overall trends of the measurement while being numerically much less demanding than a complete quantum-mechanical model [45].

A useful tool for assessing hyperfine-field distributions of organic semiconductors is magnetic resonance spectroscopy [46]. Since the linewidth of electrically detected magnetic resonance spectra of OLEDs is determined by inhomogeneous broadening due to the local hyperfine fields [14,20,29], angle-dependent magnetic-resonance experiments are expected to provide access to the combined effects of microscopic anisotropy of the hyperfine fields and macroscopic molecular ordering within the OLED. Moreover, it is even conceivable to extend the approach of magnetic resonance spectroscopy to the single-molecule level [47,48], thereby reducing inhomogeneous broadening of the resonance and opening up the ability to map out microscopic hyperfine-field distributions of molecular electronic states.

Polymer-based OLEDs evidently serve as a spectacularly sensitive inclination compass at geomagnetic field strengths, following a spin-dependent recombination mechanism not entirely dissimilar to the radical-pair process that has been put forward to rationalize the orientational abilities of certain species of migratory birds. An intriguing experimental observation in the magnetoreceptive abilities of such species is the fact that birds appear to lose their orientation when exposed to very weak oscillating magnetic fields such as those related to ambient electromagnetic noise generated, e.g., by power transformers [49,50]. An exciting challenge to extend our experimental approach and examine the relation between OLEDs and more conventional radical-pair MFEs would therefore be to investigate anisotropic MR in the presence of rf excitation, with the goal of possibly contributing to identifying microscopic mechanisms of this remarkable loss of magnetoreceptive abilities. One of the key questions in biological magnetoreception relates to the fact how tiny changes in reaction yields with magnetic field variations can be translated into physiologically perceptible signals [4]. We leave the reader to mull the fact that changes to the overall symmetry of the normalized computed magnetoresistance anisotropy are easily perceived by the naked eye in Fig. 8, on a field scale of barely 1 μT.

ACKNOWLEDGMENTS

This work is funded by the Deutsche Forschungsgemeinschaft (DFG, German Research Foundation) (Project ID No. 314695032 – SFB 1277, subproject B03). P.L.B. acknowledges support from his Australian Research Council Laureate Fellowship (Grant No. FL160100067). The National Deuteration Facility is partly funded by NCRIS, an Australian Government initiative.

[1] K. Schulten and C. E. Swenberg, A biomagnetic sensory mechanism based on magnetic field modulated coherent electron spin motion, Z. Phys. Chem. **NF 111**, 1 (1978).

[2] T. Ritz, S. Adem, and K. Schulten, A model for photoreceptor-based magnetoreception in birds, Biophys. J. **78**, 707 (2000).

[3] C. T. Rodgers and P. J. Hore, Chemical magnetoreception in birds: The radical pair mechanism, Proc. Natl. Acad. Sci. USA **106**, 353 (2009).

[4] P. J. Hore and H. Mouritsen, The radical-pair mechanism of magnetoreception, Annu. Rev. Biophys. **45**, 299 (2016).

[5] H. Mouritsen, Long-distance navigation and magnetoreception in migratory animals, Nature (London) **558**, 50 (2018).

[6] J. Xu, L. E. Jarocha, T. Zollitsch, M. Konowalczyk, K. B. Henbest, S. Richert, M. J. Golesworthy, J. Schmidt, V. Déjean, D. J. C. Sowood *et al.*, Magnetic sensitivity of cryptochrome 4 from a migratory songbird, Nature (London) **594**, 535 (2021).

[7] U. E. Steiner and T. Ulrich, Magnetic-field effects in chemical-kinetics and related phenomena, Chem. Rev. **89**, 51 (1989).

[8] B. Brocklehurst, Spin correlation in the geminate recombination of radical ions in hydrocarbons. Part 1.-Theory of the magnetic field effect, J. Chem. Soc. Faraday Trans. II **72**, 1869 (1976).

[9] E. W. Knapp and K. Schulten, Magnetic field effect on the hyperfine-induced electron spin motion in radicals undergoing diamagnetic–paramagnetic exchange, J. Chem. Phys. **71**, 1878 (1979).

[10] D. Mims, J. Herpich, N. N. Lukzen, U. E. Steiner, and C. Lambert, Readout of spin quantum beats in a charge-separated radical pair by pump-push spectroscopy, Science **374**, 1470 (2021).

[11] P. J. Hore, Radical quantum oscillations, Science **374**, 1447 (2021).

[12] T. D. Nguyen, B. R. Gautam, E. Ehrenfreund, and Z. V. Vardeny, Magnetoconductance Response in Unipolar and Bipolar Organic Diodes at Ultrasmall Fields, Phys. Rev. Lett. **105**, 166804 (2010).

[13] P. Klemm, S. Bange, A. Pöllmann, C. Boehme, and J. M. Lupton, Nanotesla magnetoresistance in π-conjugated polymer devices, Phys. Rev. B **95**, 241407(R) (2017).

[14] T. Grünbaum, S. Milster, H. Kraus, W. Ratzke, S. Kurrmann, V. Zeller, S. Bange, C. Boehme, and J. M. Lupton, OLEDs as models for bird magnetoception: Detecting electron spin resonance in geomagnetic fields, Faraday Discuss. **221**, 92 (2020).

[15] W. Wagemans, A. J. Schellekens, M. Kemper, F. L. Bloom, P. A. Bobbert, and B. Koopmans, Spin-spin Interactions in Organic Magnetoresistance Probed by Angle-Dependent Measurements, Phys. Rev. Lett. **106**, 196802 (2011).

[16] M. Cox, F. Zhu, J. M. Veerhoek, and B. Koopmans, Anisotropic magnetoconductance in polymer thin films, Phys. Rev. B **89**, 195204 (2014).

[17] F. Cintolesi, T. Ritz, C. W. M. Kay, C. R. Timmel, and P. J. Hore, Anisotropic recombination of an immobilized photoinduced radical pair in a 50-μT magnetic field: a model avian photomagnetoreceptor, Chem. Phys. **294**, 385 (2003).

[18] W. Wiltschko, U. Munro, H. Ford, and R. Wiltschko, Magnetic inclination compass: A basis for the migratory orientation of birds in the Northern and Southern Hemisphere, Experientia **49**, 167 (1993).

[19] C. Kerpal, S. Richert, J. G. Storey, S. Pillai, P. A. Liddell, D. Gust, S. R. Mackenzie, P. J. Hore, and C. R. Timmel, Chemical compass behaviour at microtesla magnetic fields strengthens the radical pair hypothesis of avian magnetoreception, Nat. Commun. **10**, 3707 (2019).

[20] D. M. Stoltzfus, G. Joshi, H. Popli, S. Jamali, M. Kavand, S. Milster, T. Grünbaum, S. Bange, A. Nahlawi, M. Y. Teferi *et al.*, Perdeuteration of poly[2-methoxy-5-(2′-ethylhexyloxy)-1,4-phenylenevinylene] (d-MEH-PPV): control of microscopic charge-carrier spin-spin coupling and of magnetic-field effects in optoelectronic devices, J. Mater. Chem. C **8**, 2764 (2020).

[21] See Supplemental Material at http://link.aps.org/supplemental/10.1103/PhysRevB.108.035201 for details on sample fabrication, a full description of numerical modeling and a critical discussion of the limitations of the model, the current dependence of the MR anisotropy, and experimental magnetoelectroluminescence anisotropy. An animation of Fig. 8 is also provided. The Supplemental Material includes Refs. [15,20,29,31–33,35,37–39,44,45,51–56].

[22] J. A. E. Wasey, A. Safonov, I. D. W. Samuel, and W. L. Barnes, Effects of dipole orientation and birefringence on the optical emission from thin films, Opt. Commun. **183**, 109 (2000).

[23] A. Graf, P. Liehm, C. Murawski, S. Hofmann, K. Leo, and M. C. Gather, Correlating the transition dipole moment orientation of phosphorescent emitter molecules in OLEDs with basic material properties, J. Mater. Chem. C **2**, 10298 (2014).

[24] M. J. Jurow, C. Mayr, T. D. Schmidt, T. Lampe, P. I. Djurovich, W. Brütting, and M. E. Thompson, Understanding and predicting the orientation of heteroleptic phosphors in organic light-emitting materials, Nat. Mater. **15**, 85 (2016).

[25] D. McBranch, I. H. Campbell, D. L. Smith, and J. P. Ferraris, Optical determination of chain orientation in electroluminescent polymer films, Appl. Phys. Lett. **66**, 1175 (1995).

[26] M. Tammer and A. P. Monkman, Measurement of the anisotropic refractive indices of spin cast thin poly(2-methoxy-5-(2′-ethyl-hexyloxy)-p-phenylenevinylene) (MEH–PPV) films, Adv. Mater. **14**, 210 (2002).

[27] O. P. Gaudin, I. D. W. Samuel, S. Amriou, and P. L. Burn, Annealing-enhanced birefringence and aggregation in MEH-PPV: A spectroscopic ellipsometry study, J. Appl. Phys. **127**, 093101 (2020).

[28] G. Giri, E. Verploegen, S. C. B. Mannsfeld, S. Atahan-Evrenk, D. H. Kim, S. Y. Lee, H. A. Becerril, A. Aspuru-Guzik, M. F. Toney, and Z. Bao, Tuning charge transport in solution-sheared organic semiconductors using lattice strain, Nature (London) **480**, 504 (2011).

[29] S. Milster, T. Grünbaum, S. Bange, S. Kurrmann, H. Kraus, D. M. Stoltzfus, A. E. Leung, T. A. Darwish, P. L. Burn, C. Boehme, and J. M. Lupton, Perdeuterated conjugated polymers for ultralow-frequency magnetic resonance of OLEDs, Angew. Chem. Int. Ed. **59**, 9388 (2020).

[30] T. D. Nguyen, G. Hukic-Markosian, F. Wang, L. Wojcik, X.-G. Li, E. Ehrenfreund, and Z. V. Vardeny, Isotope effect in spin response of pi-conjugated polymer films and devices, Nat. Mater. **9**, 345 (2010).

[31] A. J. Schellekens, W. Wagemans, S. P. Kersten, P. A. Bobbert, and B. Koopmans, Microscopic modeling of magnetic-field effects on charge transport in organic semiconductors, Phys. Rev. B **84**, 075204 (2011).

[32] N. J. Harmon and M. E. Flatté, Effects of spin-spin interactions on magnetoresistance in disordered organic semiconductors, Phys. Rev. B **85**, 245213 (2012).

[33] V. V. Mkhitaryan, D. Danilovic, C. Hippola, M. E. Raikh, and J. Shinar, Comparative analysis of magnetic resonance in the polaron pair recombination and the triplet exciton-polaron quenching models, Phys. Rev. B **97**, 035402 (2018).

[34] S. Mukamel, *Principles of Nonlinear Optical Spectroscopy* (Oxford University Press, Oxford, 1995).

[35] K. Schulten and P. G. Wolynes, Semiclassical description of electron spin motion in radicals including the effect of electron hopping, J. Chem. Phys. **68**, 3292 (1978).

[36] H. Malissa, R. Miller, D. L. Baird, S. Jamali, G. Joshi, M. Bursch, S. Grimme, J. van Tol, J. M. Lupton, and C. Boehme, Revealing weak spin-orbit coupling effects on charge carriers in a π-conjugated polymer, Phys. Rev. B **97**, 161201(R) (2018).

[37] K. J. van Schooten, D. L. Baird, M. E. Limes, J. M. Lupton, and C. Boehme, Probing long-range carrier-pair spin–spin interactions in a conjugated polymer by detuning of electrically detected spin beating, Nat. Commun. **6**, 6688 (2015).

[38] S. Kuroda, T. Noguchi, and T. Ohnishi, Electron Nuclear Double Resonance Observation of π-Electron Defect States in Undoped Poly(Paraphenylene Vinylene), Phys. Rev. Lett. **72**, 286 (1994).

[39] Y. Shimoi, S. Abe, S. Kuroda, and K. Murata, Polarons and their ENDOR spectra in poly(p-phenylene vinylene), Solid State Commun. **95**, 137 (1995).

[40] In panels (c) and (d) of Fig. 6, $\eta = 0.2$, i.e., $b_{\mathrm{hyp},\ z',\nu} = 0.2\ b_{\mathrm{hyp},\ x',\nu} = 0.2\ b_{\mathrm{hyp},\ y',\nu}$, but in contrast to the case of panels (a) and (b), Fig. 6, the z' axes are distributed isotropically. The same is found for $\eta = 4$.

[41] To quantify the relative anisotropy in the field region of fourfold symmetry, we use the expression $a' = 2\frac{\mathrm{MR}(\alpha=0^\circ)-\mathrm{MR}(\alpha=45^\circ)}{|\mathrm{MR}(\alpha=0^\circ)+\mathrm{MR}(\alpha=45^\circ)|}$, where $\mathrm{MR}(\alpha = 0^\circ)$ and $\mathrm{MR}(\alpha = 45^\circ)$ are averaged over equivalent orientations of **B**.

[42] W. J. Baker, D. R. McCamey, K. J. van Schooten, J. M. Lupton, and C. Boehme, Differentiation between polaron-pair and triplet-exciton polaron spin-dependent mechanisms in organic light-emitting diodes by coherent spin beating, Phys. Rev. B **84**, 165205 (2011).

[43] M. Kavand, D. Baird, K. van Schooten, H. Malissa, J. M. Lupton, and C. Boehme, Discrimination between spin-dependent charge transport and spin-dependent recombination in π-conjugated polymers by correlated current and electroluminescence-detected magnetic resonance, Phys. Rev. B **94**, 075209 (2016).

[44] W. J. Baker, T. L. Keevers, J. M. Lupton, D. R. McCamey, and C. Boehme, Slow Hopping and Spin Dephasing of Coulombically Bound Polaron Pairs in an Organic Semiconductor at Room Temperature, Phys. Rev. Lett. **108**, 267601 (2012).

[45] T. P. Fay, L. P. Lindoy, D. E. Manolopoulos, and P. J. Hore, How quantum is radical pair magnetoreception?, Faraday Discuss. **221**, 77 (2020).

[46] D. R. McCamey, K. J. van Schooten, W. J. Baker, S.-Y. Lee, S.-Y. Paik, J. M. Lupton, and C. Boehme, Hyperfine-Field-Mediated Spin Beating in Electrostatically Bound Charge Carrier Pairs, Phys. Rev. Lett. **104**, 017601 (2010).

[47] J. Köhler, J. A. J. M. Disselhorst, M. C. J. M. Donckers, E. J. J. Groenen, J. Schmidt, and W. E. Moerner, Magnetic resonance of a single molecular spin, Nature (London) **363**, 242 (1993).

[48] J. Wrachtrup, C. von Borczyskowski, J. Bernard, M. Orrit, and R. Brown, Optical detection of magnetic resonance in a single molecule, Nature (London) **363**, 244 (1993).

[49] T. Ritz, P. Thalau, J. B. Phillips, R. Wiltschko, and W. Wiltschko, Resonance effects indicate a radical-pair mechanism for avian magnetic compass, Nature (London) **429**, 177 (2004).

[50] S. Engels, N.-L. Schneider, N. Lefeldt, C. M. Hein, M. Zapka, A. Michalik, D. Elbers, A. Kittel, P. J. Hore, and H. Mouritsen, Anthropogenic electromagnetic noise disrupts magnetic compass orientation in a migratory bird, Nature (London) **509**, 353 (2014).

[51] M. Reufer, M. J. Walter, P. G. Lagoudakis, A. B. Hummel, J. S. Kolb, H. G. Roskos, U. Scherf, and J. M. Lupton, Spin-conserving carrier recombination in conjugated polymers, Nat. Mater. **4**, 340 (2005).

[52] G. Lindblad, On the generators of quantum dynamical semigroups, Commun. Math. Phys. **48**, 119 (1976).

[53] V. Gorini, A. Kossakowski, and E. C. Sudarsahan, Completely positive dynamical semigroups of N-level systems, J. Math. Phys. **17**, 821 (1976).

[54] A. V. Barabanov, O. V. Tretiak, and V. A. L'vov, Complete theoretical analysis of the Kaplan-Solomon-Mott mechanism of spin-dependent recombination in semiconductors, Phys. Rev. B **54**, 2571 (1996).

[55] J. E. Lawrence, A. M. Lewis, D. E. Manolopoulos, and P. J. Hore, Magnetoelectroluminescence in organic light-emitting diodes, J. Chem. Phys. **144**, 214109 (2016).

[56] M. Pope and C. E. Swenberg, *Electronic Processes in Organic Crystals and Polymers*, 2nd ed. (Oxford University Press, New York, 1999).